Dual-pulse nonlinear photoacoustic technique: a practical investigation

Chao Tian,[1] Zhixing Xie,[1,*] Mario L. Fabiilli,[1] Shengchun Liu,[1,2] Cheng Wang,[3] Qian Cheng,[4] and Xueding Wang[1]

[1]*Department of Radiology, University of Michigan, Ann Arbor, MI 48109, USA*
[2]*College of Physical Science and Technology, Heilongjiang University, Harbin, 150080, China*
[3]*School of Medical Instrument and Food Engineering, University of Shanghai for Science and Technology, Shanghai 200093, China*
[4]*Institute of Acoustics, Tongji University, Shanghai 200092, China*
[*]*zhixing@umich.edu*

Abstract: The dual-pulse nonlinear photoacoustic technique is a recently developed technology based on temperature dependence of the Grüneisen parameter and involves consecutive excitations of biological tissue using two laser pulses with a short time delay. Here we review the principle of the technique and give a discussion about its technical aspects, including selection and combination of excitation laser wavelengths, determination of laser fluence, estimation of thermal relaxation function and probability of photoablation or cavitation. Comparisons between the dual-pulse technique and conventional photoacoustics as well as thermal photoacoustics are also presented. These investigations are supported by experimental results and will give a practical reference and guide for further developments of the technique.

References and links

1. M. Xu and L. V. Wang, "Photoacoustic imaging in biomedicine," Rev. Sci. Instrum. **77**(4), 041101 (2006).
2. C. Li and L. V. Wang, "Photoacoustic tomography and sensing in biomedicine," Phys. Med. Biol. **54**(19), R59–R97 (2009).
3. L. V. Wang, "Multiscale photoacoustic microscopy and computed tomography," Nat. Photonics **3**(9), 503–509 (2009).
4. X. Wang, Y. Pang, G. Ku, X. Xie, G. Stoica, and L. V. Wang, "Noninvasive laser-induced photoacoustic tomography for structural and functional in vivo imaging of the brain," Nat. Biotechnol. **21**(7), 803–806 (2003).
5. Z. Xie, S. Jiao, H. F. Zhang, and C. A. Puliafito, "Laser-scanning optical-resolution photoacoustic microscopy," Opt. Lett. **34**(12), 1771–1773 (2009).
6. Z. Xie, C. Tian, S.-L. Chen, T. Ling, C. Zhang, L. J. Guo, P. L. Carson, and X. Wang, "3D high resolution photoacoustic imaging based on pure optical photoacoustic microscopy with microring resonator," in SPIE BiOS, (International Society for Optics and Photonics, 2014), 894314.
7. L. V. Wang and H.-i. Wu, *Biomedical Optics: Principles and Imaging* (John Wiley & Sons, 2007).
8. S. Pramuditya, "Water Thermodynamic Properties" (2011), retrieved 09/13, 2014, *http://syeilendrapramuditya.wordpress.com/2011/08/20/water-thermodynamic-properties/*.
9. V. A. Del Grosso and C. W. Mader, "Speed of Sound in Pure Water," J. Acoust. Soc. Am. **52**(5B), 1442–1446 (1972).
10. F. A. Duck, *Physical Properties of Tissues: A Comprehensive Reference Book* (Academic Press, 1990).
11. V. P. Zharov, K. E. Mercer, E. N. Galitovskaya, and M. S. Smeltzer, "Photothermal nanotherapeutics and nanodiagnostics for selective killing of bacteria targeted with gold nanoparticles," Biophys. J. **90**(2), 619–627 (2006).
12. J. Shah, L. Ma, K. Sokolov, K. Johnston, T. Milner, S. Y. Emelianov, S. Park, S. Aglyamov, and T. Larson, "Photoacoustic imaging and temperature measurement for photothermal cancer therapy," J. Biomed. Opt. **13**, 034024 (2008).
13. Y. S. Chen, W. Frey, C. Walker, S. Aglyamov, and S. Emelianov, "Sensitivity enhanced nanothermal sensors for photoacoustic temperature mapping," J. Biophotonics **6**(6-7), 534–542 (2013).
14. D. Yeager, Y.-S. Chen, S. Litovsky, and S. Emelianov, "Intravascular photoacoustics for image-guidance and temperature monitoring during plasmonic photothermal therapy of atherosclerotic plaques: a feasibility study," Theranostics **4**(1), 36–46 (2014).

15. J. Yao, H. Ke, S. Tai, Y. Zhou, and L. V. Wang, "Absolute photoacoustic thermometry in deep tissue," Opt. Lett. **38**(24), 5228–5231 (2013).
16. S.-H. Wang, C.-W. Wei, S.-H. Jee, and P.-C. Li, "Photoacoustic temperature measurements for monitoring of thermal therapy," Photons Plus Ultrasound: Imaging and Sensing **2009**, 7177 (2009).
17. L. Wang, C. Zhang, and L. V. Wang, "Grueneisen relaxation photoacoustic microscopy," Phys. Rev. Lett. **113**(17), 174301 (2014).
18. P. Lai, L. Wang, J. W. Tay, and L. V. Wang, "Photoacoustically guided wavefront shaping for enhanced optical focusing in scattering media," Nat. Photonics **9**(2), 126–132 (2015).
19. C. Tian, Z. Xie, M. L. Fabiilli, and X. Wang, "Imaging and sensing based on dual-pulse nonlinear photoacoustic contrast: a preliminary study on fatty liver," Opt. Lett. **40**(10), 2253–2256 (2015).
20. I. V. Larina, K. V. Larin, and R. O. Esenaliev, "Real-time optoacoustic monitoring of temperature in tissues," J. Phys. D Appl. Phys. **38**(15), 2633–2639 (2005).
21. S. L. Jacques, "Optical properties of biological tissues: a review," Phys. Med. Biol. **58**(11), R37–R61 (2013).
22. S. Prahl, R. L. P. v. Veen, H. J. C. M. Sterenborg, A. Pifferi, A. Torricelli, and R. Cubeddu, "Optical Properties Spectra", retrieved 09/13, 2014, *http://omlc.org/spectra/*.
23. S. Ashkenazi, "Photoacoustic lifetime imaging of dissolved oxygen using methylene blue," J. Biomed. Opt. **15**, 040501 (2010).
24. B. Cox, "Introduction to laser-tissue interactions," PHAS **4886**, 1–61 (2007).
25. P. Beard, "Biomedical photoacoustic imaging," Interface focus, rsfs20110028 (2011).
26. R. S. Dingus and R. J. Scammon, "Grüneisen-stress-induced ablation of biological tissue," in *Optics, Electro-Optics, and Laser Applications in Science and Engineering*, (International Society for Optics and Photonics, 1991), 45–54.
27. G. Paltauf, E. Reichel, and H. Schmidt-Kloiber, "Study of different ablation models by use of high-speed-sampling photography," in OE/LASE'92, (International Society for Optics and Photonics, 1992), 343–352.
28. G. Paltauf, H. Schmidt-Kloiber, and M. Frenz, "Photoacoustic waves excited in liquids by fiber-transmitted laser pulses," J. Acoust. Soc. Am. **104**(2), 890–897 (1998).
29. T. L. Szabo, *Diagnostic Ultrasound Imaging: Inside Out* (Elsevier Academic Press, 2004).
30. G. Paltauf and H. Schmidt-Kloiber, "Microcavity dynamics during laser-induced spallation of liquids and gels," Appl. Phys., A Mater. Sci. Process. **62**(4), 303–311 (1996).
31. A. A. Oraevsky, S. L. Jacques, and F. K. Tittel, "Mechanism of laser-ablation for aqueous-media irradiated under confined-stress conditions," J. Appl. Phys. **78**(2), 1281–1290 (1995).
32. S. L. Jacques, G. Gofstein, and R. S. Dingus, "Laser-flash photography of laser-induced spallation in liquid media," in OE/LASE'92, (International Society for Optics and Photonics, 1992), 284–294.

1. Introduction

Photoacoustic imaging (PAI), which uses a pulsed laser to excite ultrasonic waves in biological tissue, is an emerging noninvasive biomedical imaging modality [1–4]. It combines two imaging modalities, i.e., optical imaging and ultrasonic imaging, and inherits both of their advantages, such as high contrast, excellent resolution and outstanding depth-resolution ratio and, therefore, has been explored extensively for its applications in biomedicine [4–6].

In PAI, the initial acoustic pressure p_0 after laser excitation can be written as [7]

$$p_0 = \Gamma \mu_a \Phi, \qquad (1)$$

where Φ is the laser fluence, μ_a is the absorption coefficient of the chromophore. Γ is the Grüneisen parameter of tissue, which is a dimensionless factor proportional to the fraction of deposited thermal energy converted into mechanical stress and is expressed as

$$\Gamma = \beta v_s^2 / C_p, \qquad (2)$$

where β is the thermal expansion coefficient, v_s is the speed of sound and C_p is the specific heat capacity at constant pressure. Due to temperature dependence nature of β, v_s and C_p, the Grüneisen parameter Γ is highly temperature-dependent and so is the photoaocustic signal p_0 [Eq. (1)]. To investigate how Γ and p_0 changes with temperature, two things need to be taken into consideration. First, comparing with v_s and C_p, β varies more significantly with temperature rise and makes the greatest contribution to the change of Grüneisen parameter Γ. Taking water as an example, from 20°C to 40°C, β increases by about 97% (from 2.3×10^{-4}/°C to 4.5×10^{-4}/°C [8]), while v_s and C_p changes by less than 4% and 1% (v_s from 1482 m/s to 1529 m/s [8, 9] and C_p from 4.185 kJ/kg·°C to 4.178 kJ/kg·°C [8]), respectively. That is to say, for a limited temperature range (several °C), it follows $p_0 \propto \Gamma \propto \beta$. Second, for different biological tissues, the change rate of β with temperature differs. For example, from

15°C to 40°C, the thermal expansion coefficient β of blood increases from $2.5 \times 10^{-4}/°C$ to $4 \times 10^{-4}/°C$ while that of lipid decreases from $19.9 \times 10^{-4}/°C$ to $9.2 \times 10^{-4}/°C$ [10]. This indicates the change of Grüneisen parameter of blood with temperature rise is positive while that of lipid is negative. These features enable thermal photoacoustics a very good tool for tissue differentiation (e.g., lipid-rich and blood-rich tissues) and temperature monitoring [11–16].

Recently, Wang and associates for the first time studied the nonlinear photoacoustic effect when two closely adjacent laser pulses are applied on the same biological tissue [17, 18]. The technique uses a short-duration pulsed laser instead of conventional heating methods (such as high-intensity focused ultrasound, or continuous wave laser) to heat the sample. Specifically, the technique first fires a short-duration pulse to heat the sample and cause a moderate temperature jump, and then uses a closely followed second pulse to measure the temperature-induced change of the Grüneisen parameter. Based on the dual-pulse technique and temperature- and tissue-dependence of the Grüneisen parameter, we developed a dual-pulse nonlinear photoacoustic contrast for fast tissue characterization [19]. The new contrast is sensitive to biochemical contents of tissue and has been demonstrated to be successful in the diagnosis of fatty liver disease.

In the dual-pulse nonlinear photoacoustic technique, several technical problems and variables, such as laser wavelength, laser fluence, time delay between the two pulses, are involved, which make it difficult to implement in experiment. The aim of this paper is to investigate practical aspects of the technique and provide useful references for future developments.

2. Principle and implementation of the dual-pulse technique

The dual-pulse technique employs a pulsed heating laser and a pulsed detecting laser to consecutively excite biological tissue with a designed time delay. For the geometric relation between the transducer and the sample in Fig. 1, the established initial acoustic pressure after the heating pulse is

$$p_0 = \Gamma \mu_a(\lambda_1)\Phi_1(x,y,z;\lambda_1;t_1), \tag{3}$$

where Φ_1 and λ_1 are the fluence and wavelength of the heating laser at time t_1. The initial wave propagates outwards and is received by the acoustic transducer. The voltage output V_1 of the received signal involves a double integration (over acoustic source S and transducer surface Σ) and can be written as

$$
\begin{aligned}
V_1 &= \eta \iint_{\Sigma} G(\xi,\zeta) \left(\iiint_S f(x,y,z;\xi,\zeta)\Gamma_0\mu_a(\lambda_1)\Phi_1(x,y,z;\lambda_1;t_1)\mathrm{d}x\mathrm{d}y\mathrm{d}z \right)\mathrm{d}\xi\mathrm{d}\zeta \\
&= \eta\Gamma_0\mu_a(\lambda_1) \cdot \iint_{\Sigma} G(\xi,\zeta) \left(\iiint_S f(x,y,z;\xi,\zeta)\Phi_1(x,y,z;\lambda_1;t_1)\mathrm{d}x\mathrm{d}y\mathrm{d}z \right)\mathrm{d}\xi\mathrm{d}\zeta \quad (4) \\
&= \eta\Gamma_0\mu_a(\lambda_1)F(\Phi_1),
\end{aligned}
$$

where η is a constant coefficient, G is an apodization function of the transducer, f is a propagating factor (including a spherical wave propagating term and an attenuation term) for acoustic waves from the source S to the transducer surface Σ, (x, y, z) and (ξ, ζ, z) are corresponding coordinates for S and Σ, respectively. The induced temperature rise ΔT after the deposition of the heating pulse can be estimated by

$$\Delta T = \frac{\mu_a\Phi}{\rho C_v}, \tag{5}$$

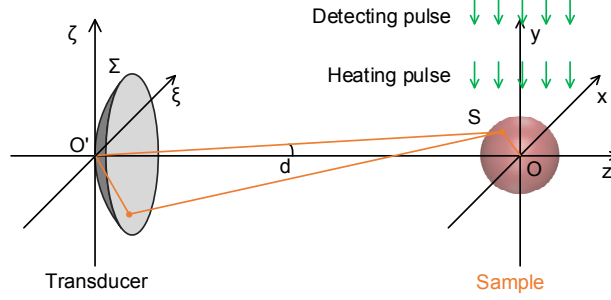where ρ and C_v are density and specific heat capacity at constant volume, respectively.

Fig. 1. Geometry of the acoustic transducer Σ and the photoacoustic source S.

Due to finite size of the heated volume, it takes time for it to cool down. Therefore, the temperature-dependent Grüneisen parameter Γ can be written as [20]

$$\Gamma(T_0 + \Delta T; \Delta t) = \Gamma_0 + \Gamma' \cdot \Delta T \cdot \tau(\Delta t), \tag{6}$$

where T_0 and Γ_0 are the baseline temperature and Grüneisen parameter, respectively, Γ' is the change slope of Γ, $\tau(\Delta t)$ is the thermal relaxation function. When the detecting laser arrives, the output signal V_2' of the transducer is

$$V_2' = \eta \Gamma_0 \mu_a(\lambda_2) F(\Phi_2) + \eta \left\{ \left[\Gamma' \cdot \frac{\mu_a(\lambda_1)}{\rho C_v} \cdot \tau(\Delta t) \right] \mu_a(\lambda_2) \right\} F(\Phi_1 \Phi_2), \tag{7}$$

where Φ_2 and λ_2 are the fluence and the wavelength of the detecting laser, respectively. For comparison, the signal of the detecting laser without the heating pulse is

$$V_2 = \eta \Gamma_0 \mu_a(\lambda_2) F(\Phi_2). \tag{8}$$

The amplitude change of the photoacoustic signal [Fig. 2(b)] due to the first heating pulse is

$$\Delta V_2 = V_2' - V_2 = \eta \left\{ \left[\Gamma' \cdot \frac{\mu_a(\lambda_1)}{\rho C_v} \cdot \tau(\Delta t) \right] \mu_a(\lambda_2) \right\} F(\Phi_1 \Phi_2). \tag{9}$$

Considering the amplitude difference ΔV_2 changes nonlinearly with the variation of laser fluence Φ_1 and Φ_2 (e.g., $\Delta V_2 \propto \Phi^2$ if $\Phi_1 = \Phi_2 = \Phi$) [17, 18], we get the nonlinear effect

$$\alpha = \frac{\Delta V_2}{V_2} = \frac{\Gamma'}{\Gamma_0} \frac{\mu_a(\lambda_1)}{\rho C_v} \tau(\Delta t) \frac{F(\Phi_1 \Phi_2)}{F(\Phi_2)}. \tag{10}$$

Further, using the derivative of Eq. (2), the nonlinear effect can be written in a more specific form, that is,

$$\alpha = \overbrace{\left(\frac{\beta'}{\beta_0} + 2 \frac{v_s'}{v_{s0}} - \frac{C_p'}{C_{p0}} \right) \frac{\mu_a(\lambda_1)}{\rho C_v}}^{\text{Tissue parameters}} \overbrace{\tau(\Delta t)}^{\text{Relaxation function}} \overbrace{\frac{F(\Phi_1 \Phi_2)}{F(\Phi_2)}}^{\text{Laser fluence}}, \tag{11}$$

where β', v_s' and C_p' are first-order derivatives of β, v_s and C_p with temperature, respectively. The above equation indicates that the nonlinear effect α is simultaneously determined by physical properties (β', v_s', C_p' and μ_a) of the tissue, relaxation function (τ) and exposed laser fluence (Φ_1 and Φ_2).

The dual-pulse technique can be summarized as follows (Fig. 2). A first laser pulse diffuses into the tissue, deposits a certain amount of laser energy Φ_1, and causes a temperature jump ΔT. Physical properties of the tissue (especially the thermal expansion coefficient β)

change due to the induced temperature jump, and affect the value of the Grüneisen parameter Γ, which is closely related to the initial photoacoustic pressure p_0. The change in p_0 leads to amplitude variation (ΔV_2) of the second photoacoustic signal, and finally generates the nonlinear effect α.
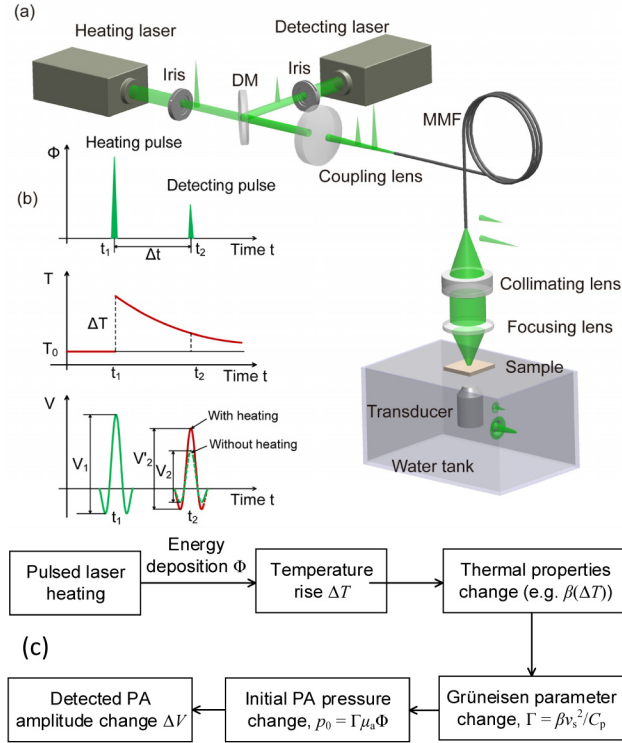

Fig. 2. Setup (a) and principle [(b) and (c)] of the dual-pulse nonlinear photoacoustic technique. DM: dichroic mirror; MMF: multi-mode fiber.

An experiemental system was built to investigate the nonlinear effect [Fig. 2(a)]. The system sequentially triggers two 532 nm lasers to create two closely accompanying pulses by a delay generator (DG535, Standford Research Systems Inc.). The first laser is a second harmonic output of a Nd:YAG laser (Powerlite DLS 8000, Continuum; pulse duration 6 ns, repetition rate 10 Hz), and works as the heating source. The second laser is also a second harmonic output of an Nd:YAG pulsed laser (Brilliant B, Quantel; pulse duration 5 ns, repetition rate 10 Hz) and works as the detecting source. After passing the irises, the two lasers are combined by a beam splitter (BSW16, Thorlabs) and then coupled into a multi-mode fiber (FG910LEC, Thorlabs; numerical aperture 0.22, core diameter 0.91 mm) by an aspheric lens (KPA031, Newport). The output port of the fiber is imaged onto the sample by a lens assembly consisting of a collimating lens (AC254-050-A, Thorlabs; focal length 50 mm) and a focusing lens (AC254-050-A, Thorlabs; focal length 50 mm). The photoacoustic signals are received by a transducer (C323, Olympus NDT, center frequency 2.25 MHz, −6 dB bandwidth 76.7%), amplified by a pulser and receiver (5072R, Olympus NDT) and finally digitized and recorded by an oscilloscope (TDS 540A, Tektronix).

The nonlinear effect was first investigated and verified on red ink (Dakota Red, Private reserve ink; $\mu_a(532 \text{ nm}) = 2400 \text{ cm}^{-1}$) at room temperature 22°C using the setup in Fig. 2. One typical experimental result is shown in Fig. 3(a), in which the blue and the red curves (see inset) are recorded photoacoustic signals without and with the heating laser, respectively. As we can see, amplitude of the second signal with heating significantly increases by ~148% (from 0.23 V to 0.57 V) compared to that without heating. Considering the Grüneisen

parameter linearly proportional to the temperature (for water, $\Gamma = 0.0043 + 0.0053T$ [7]), the induced temperature rise ΔT is estimated to be about 38°C and the predicted laser fluence is about 63 mJ/cm^2 [Eq. (5)]. Figure 3(b) shows several successive measurements, which shows the nonlinear effect is pretty stable.
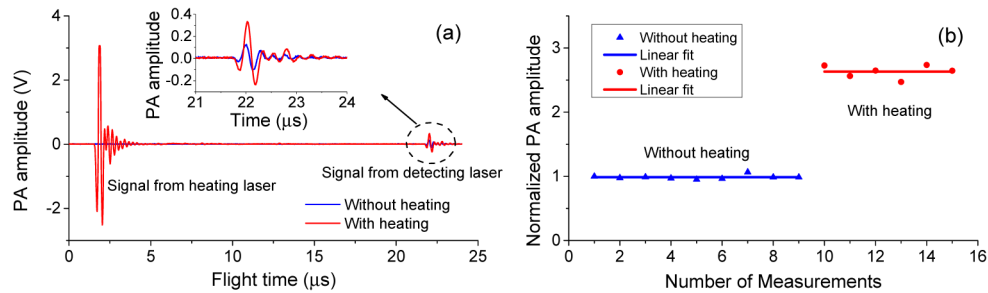

Fig. 3. Experimental measurement of the nonlinear effect of red ink. (a) Photoacoustic signals of the detecting laser without and with heating (see inset for detail); (b) Normalized amplitude of the detecting photoacoustic signal without and with heating in several consecutive measurements.

3. Practical investigations of the dual-pulse technique

To apply the dual-pulse technique in biomedical imaging, stable, repeatable and controllable nonlinear effect is a necessity, which is, however, affected by many factors. In this Section, we will discuss these influential parameters, including thermal properties of tissue (i.e. Grüneisen parameter), excitation laser wavelength, laser fluence, thermal relaxation function as well as possible undesirable effects (e.g., cavitation), and give a useful guide for practical implementation of the technique.

3.1 Combination and selection of excitation laser wavelengths

Temperature dependence of the physical parameters of biological tissue is the basis of the dual-pulse technology. Greater dependence produces higher nonlinear effect and better contrast. It is fortunate that most physical parameters of tissue have strong dependence on temperature [21]. This makes it possible to find potential applications of the dual-pulse technique.

Besides thermal properties, combination and selection of excitation laser wavelengths are also very important. Two aspects are considered here. The first is the combination of heating and detecting laser wavelengths. This is important because it determines the geometrical size relation of the heated volume U_1 and the detected volume U_2 of the tissue. Since different wavelengths λ mean different absorption coefficients μ_a, the problem can be further divided into three subcases, i.e., $\mu_a(\lambda_1) = \mu_a(\lambda_2)$, $\mu_a(\lambda_1) < \mu_a(\lambda_2)$ and $\mu_a(\lambda_1) > \mu_a(\lambda_2)$. The first subcase is regular and the simplest, and indicates both the wavelengths λ and penetration depths δ of the two lasers are the same ($\lambda_1 = \lambda_2$ and $\delta_1 = \delta_2$). The detected volume U_2 completely overlaps the heated volume U_1 (i.e., $U_2 = U_1$), and all heated voxels in U_1 contribute to the final nonlinear effect α. The second subcase indicates a combination of different wavelengths ($\lambda_1 \neq \lambda_2$), and the penetration depth of the heating laser δ_1 is greater than that of the detecting laser δ_2 ($\delta_1 > \delta_2$). For this situation, the detected volume U_2 is completely embedded in the heated volume U_1 (i.e., $U_2 \subset U_1$) and the nonlinear effect α may be high but with certain amount of deposited energy loss. The last subcase also indicates a combination of different wavelengths ($\lambda_1 \neq \lambda_2$), but the heating laser has a smaller penetration depth δ_1 than that of the detecting laser δ_2 ($\delta_1 < \delta_2$). For this situation, the heated volume U_1 is only part of the detected volume U_2 (i.e., $U_1 \subset U_2$) and the induced nonlinear effect α may be low. The three subcases are summarized as below:

1) $\lambda_1 = \lambda_2$, $\mu_a(\lambda_1) = \mu_a(\lambda_2)$, $\delta_1 = \delta_2$ and $U_1 = U_2$, most efficient combination;

2) $\lambda_1 \neq \lambda_2$, $\mu_a(\lambda_1) < \mu_a(\lambda_2)$, $\delta_1 > \delta_2$ and $U_1 \supset U_2$, higher nonlinear effect;

3) $\lambda_1 \neq \lambda_2$, $\mu_a(\lambda_1) > \mu_a(\lambda_2)$, $\delta_1 < \delta_2$ and $U_1 \subset U_2$, lower nonlinear effect.

In experiment, the ideal situations should be the first two, i.e., $\mu_a(\lambda_1) \leq \mu_a(\lambda_2)$, which guarantees optimum nonlinear effect α.

The second aspect involves the selection of the specific heating wavelength λ_1. This is important because it relates to the absorption coefficient μ_a, which determines the deposited energy density $\mu_a\Phi_1$ (unit: mJ/cm³). In other words, it determines the induced temperature jump ΔT for a given heating laser fluence Φ_1 [Eq. (5)]. The higher the absorption coefficient μ_a, the greater the temperature jump ΔT and the stronger the nonlinear effect α. In practice, it is critical to tune the heating laser wavelength λ_1 to one of the absorption peaks of the target chormophores (e.g., 532 nm for blood, 1210 nm or 1720 nm for lipid in Fig. 4) to enable efficient heating as well as detecting.
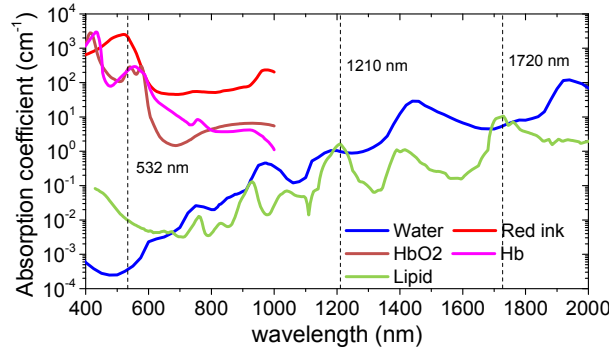

Fig. 4. Optical absorption spectra of water, red ink, oxygenated (HbO2) and deoxygenated (Hb) blood and lipid [22]. The spectrum of red ink was measured using spectrophotometer (SpectraMax Plus 384, Molecular Devices, LLC).

3.2 Determination of laser fluence

To determine the correct fluence of heating laser Φ_1 and probing laser Φ_2 in the experiment, we need to investigate the relations between them and the nonlinear effect. Considering Eq. (4) and the last term of Eq. (11), the relation can be mathematically described as

$$\frac{F(\Phi_1\Phi_2)}{F(\Phi_2)} = \frac{\iint_\Sigma G(\xi,\zeta)\left(\iiint_s f(x,y,z;\xi,\zeta)\Phi_1(x,y,z;\lambda_1;t_1)\Phi_2(x,y,z;\lambda_2;t_2)\mathrm{d}x\mathrm{d}y\mathrm{d}z\right)\mathrm{d}\xi\mathrm{d}\zeta}{\iint_\Sigma G(\xi,\zeta)\left(\iiint_s f(x,y,z;\xi,\zeta)\Phi_2(x,y,z;\lambda_2;t_2)\mathrm{d}x\mathrm{d}y\mathrm{d}z\right)\mathrm{d}\xi\mathrm{d}\zeta}. \quad (12)$$

The above equation shows that, although the amplitude change ΔV_2 increases nonlinearly with the product of Φ_1 and Φ_2 [Eq. (11)], the nonlinear effect α is only linearly proportional to the heating laser fluence Φ_1 (e.g., $2\Phi_1$ corresponding to 2α) and independent on the detecting laser fluence Φ_2 (e.g., $2\Phi_2$ still corresponding to α) .

To verify this, we independently studied the two relations using the setup in Fig. 2. The sample used was human whole blood (from the University of Michigan hospital blood bank), which was kept flowing through a plastic tube during the experiment. The time interval Δt between the two laser pulses was 20 μs. Figure 5(a) shows that, for fixed detecting laser fluence Φ_2, the nonlinear effect α increases linearly with the growth of heating laser fluence Φ_1, whereas Fig. 5(b) illustrates that, for fixed Φ_1, α almost remains the same with the growth of Φ_2. The results agree with the theoretical predications very well and give us good references on how to properly balance the fluences of the two lasers. That is to say, the heating laser fluence Φ_1 can be increased to enhance the nonlinear effect α, while the detecting laser fluence Φ_2 can be depressed to avoid excessive laser exposure.
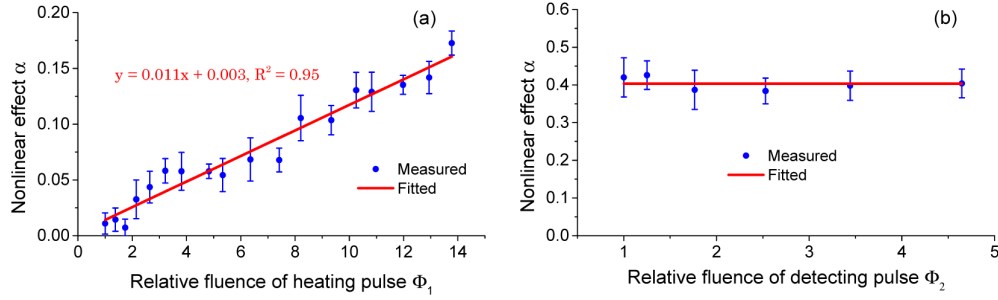
Fig. 5. Relations between the nonlinear effect and the fluences of the heating laser (a) and the detecting laser (b).

3.3 Estimation of thermal relaxation function

When a target is heated, it will transfer its heat to surrounding tissues, but the process generally takes some time. The time required for the target to cool to 50% of its peak temperature is the thermal relaxation time τ_{th}, which relates to the target diameter d through the expression

$$\tau_{th} = d^2 / \alpha_{th},$$ (13)

where α_{th} is the thermal diffusivity and approximately equals 0.13 mm²/s for soft tissue [7]. For an object with a diameter $d = 10$ μm, the thermal confinement time τ_{th} is estimated to be ~770 μs.

Temperature decay also occurs in the dual-pulse technique just after the irradiance of the heating laser. This indicates the magnitude of the nonlinear effect α will decrease if the time interval Δt between the two lasers becomes larger, and the decay is exponential. To achieve reasonable nonlinear effect, the detecting laser should arrive within the thermal relaxation time (i.e., $\Delta t \leq \tau_{th}$), i.e., satisfying the thermal confinement condition. We verified the decay process of the nonlinear effect using the setup in Fig. 2.

The sample used was also human whole blood but on a thin plastic membrane. The fluences of the two lasers Φ_1 and Φ_2 remain unchanged during the experiment. Figure 6 shows the experimental result, which indicates that the nonlinear effect α decreases with the increase of the time interval Δt between the two lasers. After exponential fitting, the normalized thermal relaxation function for this case is

$$\tau(\Delta t) = \exp(-7.9 \times 10^{-3} \Delta t).$$ (14)

The thermal relaxation time τ_{th} and the diameter d of the heated region are estimated to be 88 ms and 0.1 mm, respectively.

The fitting coefficient (i.e., -7.9×10^{-3}) in Eq. (14) has a physical dimension ms⁻¹ and indicates thermal diffusion rate of the target tissue. The bigger the value is, the faster the target cools down. From this perspective, the dual-pulse technique has the potential for measuring some very basic physical quantities, such as thermal diffusivity. This feature makes it very similar to photoacoustic lifetime imaging (PALI), which also uses a pump-probe strategy and measures decay process of some lifetime events, such as tissue oxygen level [23].
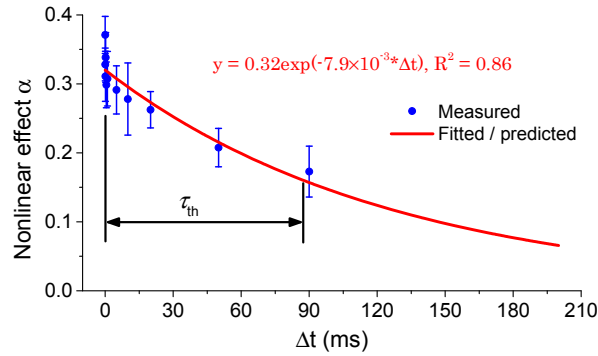
Fig. 6. Measured and fitted thermal relaxation function.

3.4 Cavitation issue

In Fig. 3, we showed the nonlinear effect of red ink measured in the experiment was as high as 148% and the estimated final temperature was about 60°C. One may wonder whether it is possible to further improve it by increasing the fluence of the heating laser Φ_1 as long as the final temperature is below the boiling point 100°C. More clearly, from 20°C to 90°C, the Grüneisen parameter of water increases by about 2.4 times and the expected nonlinear effect α should be as high as 240% [7]. We tried to achieve this in experiment, but found it is quite difficult.

To find out the reason and what happened in the experiment, it is helpful for us to understand different laser-tissue interaction mechanisms. Figure 7 shows five commonly recognized laser-tissue interaction mechanisms according to laser exposure time and irradiance, i.e. photochemistry, photothermal, photoablation, plasma-induced photoablation, and photodisruption [24]. PAI generally employs a nanosecond timescale laser (to meet the stress confinement condition) to excite the tissue and uses a low laser fluence (usually < 20 mJ/cm^2) to induce small temperature rises (< 0.1°C) [25]. Its working regime belongs to the photothermal range (Fig. 7), in which thermal conversion is the dominant effect. However, to achieve greater temperature jump, the dual-pulse nonlinear photoacoustic technique requires higher laser fluence Φ_1 (usually several hundred mJ/cm^2) [18], which pushes the technique towards the regime of photoablation (Fig. 7). In other words, sample in nonlinear photoacoustics may be ablated if the laser fluence Φ_1 is too high. Tissue ablation by laser is a complex process, which involves several mechanisms, such as photothermal decomposition and spallation (cavitation) [26]. Photothermal decomposition generally requires high temperature (> 100°C) to cause explosive vaporization of tissue and will not happen in the dual-pulse technique. However, cavitation, a mechanical effect caused by negative stress waves, is likely to occur even the temperature jump ΔT is low.
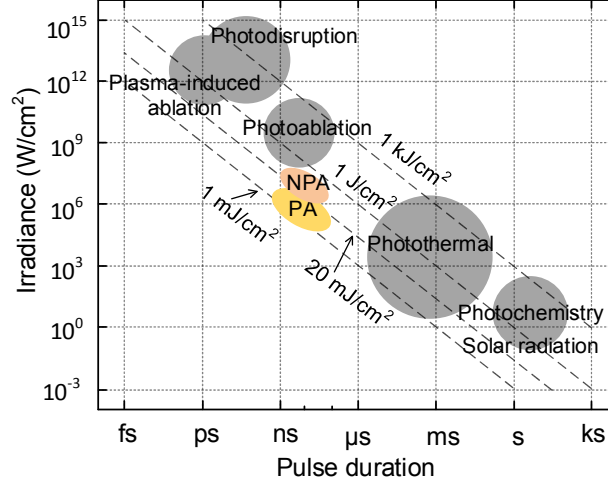
Fig. 7. Different laser-tissue interaction mechanisms in logarithmic scale (both axes) [24].

Although initial photoacoustic signals are compressive waves, subsequent propagation of these waves may result in both compressive and tensile stresses (negative pressure) due to reflection of the compressive waves from a boundary with acoustic impedance mismatch (such as tissue-air interface) [27] or three-dimensional characteristics of wave propagation [28]. Once generated, the tensile stresses will cause cavitation in the sample which degrades energy conversion efficiency from light to heat due to the generation of acoustic bubbles. Considering a sample (e.g., blood), which has an absorption coefficient μ_a = 240 cm^{-1} at 532 nm, is placed on the surface of water with air on the top (i.e., water-blood-air, $+ z$ perpendicular to the surface and towards air) and irradiated by a laser with a fluence Φ_1 = 500 mJ·cm^{-2}, the initial photoacostic pressure

$$p_0 = \Gamma \mu_a \Phi_1 = 0.20 \times 240 \text{cm}^{-1} \times 500 \text{mJ} \cdot \text{cm}^{-2} = 24 \text{MPa}, \tag{15}$$

where Γ = 0.20 for blood at 37°C. The generated compressive pressure propagates towards both the air ($+ z$) and the water (-z). Due to the mismatch of acoustic impedance at the blood-air interface, the $+ z$ component will be reflected and inverted in phase and become tensile waves, which follows the tail of the -z component and forms a bipolar wave. The amplitude of the tensile waves is half of that of the initial pressure, that is,

$$p_{\text{neg}} = p_0 / 2 = 12 \text{MPa}. \tag{16}$$

Since the center frequency f_c of the transducer is 2.25 MHz, the corresponding mechanical index (MI) [29], which is used to measure the ultrasound-induced bioeffect, is

$$\text{MI} = \frac{p_{\text{neg}}}{\sqrt{f_c}} = 8. \tag{17}$$

This has far exceeded the US Food and Drug Administration (FDA) regulated value 1.9 [29], and is very likely to induce cavitation in the sample [30–32].

Using the safty limit MI = 1.9, the greatest negative pressure p_{neg} is about 2.9 MPa and the maximum allowable laser fluence

$$\Phi_{1\text{max}} = \frac{2 p_{\text{neg}}}{\Gamma \mu_a} = \frac{2 \times 2.9 \times 10^6 \text{Pa}}{0.2 \times 240 \text{cm}^{-1}} = 121 \text{mJ} \cdot \text{cm}^{-2}. \tag{18}$$

The maximum temperature jump

$$\Delta T_{max} = \frac{\mu_a \Phi_{1max}}{\rho C_v} = \frac{240 \text{cm}^{-1} \times 121 \text{mJ} \cdot \text{cm}^{-2}}{1 \text{g} \cdot \text{cm}^{-3} \times 4 \text{J} \cdot \text{g}^{-1} \cdot \text{K}^{-1}} = 7.3 \text{K}. \qquad (19)$$

Recalling the empirical formula of the Grüneisen parameter of water with temperature, the maximum nonlinear effect α is expected to be 19% (at body temperature 37°C). Reducing the heating laser fluence Φ_1 helps decrease the probability of cavitation, but the nonlinear effect α will also be surpressed. One method to prevent or ease the occurrence of cavitation is to avoid acoustic impedance mismatch, because the generation of negative pressure depends greatly on boundary conditions. This can be done by completely submerging the sample into water or just using a very thin layer of samples.

Although the estimated maximum nonlinear effect without cavitation is estimated to be only 19%, this does not mean it cannot be further improved. Higher nonlinear effect is still achievable using higher laser fluence, but the efficiency will be lower because of energy loss due to mechanical energy conversion. For most experimental systems, 19% nonlinear effect already gives enough dynamic range, which ensures the applicability of the technique.

4. Conclusion

The dual-pulse nonlinear photoacoustic technique is a novel idea built on the physics of thermal photoacoustics (i.e., temperature dependence of Grüneisen parameter) but with higher temperature rise (tens of degrees) and shorter heating time (nanosecond timescale).

We reviewed the principle of the technique and investigated its several practical aspects, i.e., wavelength combination and selection, laser fluence, relaxation function and potential possibility of ablation (cavitation). From the viewpoint of maximum heating efficiency, the absorption coefficient of heating laser $\mu_a(\lambda_1)$ should be at absorption peaks of the tissue and as high as possible. From the perspective of maximum probing efficiency, the absorption coefficient of detecting laser $\mu_a(\lambda_2)$ should be no smaller than that of heating laser $\mu_a(\lambda_1)$ [i.e., $\mu_a(\lambda_2) > \mu_a(\lambda_1)$] (Section 3.1). The most important technical indicator, the nonlinear effect, is linearly proportional to the heating laser fluence Φ_1, but independent on the detecting laser fluence Φ_2 (Section 3.2, Fig. 5). This helps us achieve the highest nonlinear effect using the lowest laser fluence. The time interval Δt between the two consecutive lasers should be within the thermal confinement time τ_{th} to avoid dissipation of the induced temperature rise ΔT (Section 3.3). If possible, the value should also be large enough to make the two photoacoustic signals separable in time.

Compared with regular photoacoustics that uses a relatively low laser fluence (usually < 20 mJ/cm^2), the dual-pulse nonlinear photoacoustics generally employs a higher one (usually several hundred mJ/cm^2). This makes it vulnerable to the occurrence of cavitation. To avoid this, the exposed laser fluence should be kept as low as possible, and the maximum nonlinear effect α_{max} for blood is expected to be about 19% (Section 3.4). This value has already exceeded the sensitivity of most systems and should give enough resolution for workable biomedical imaging [19]. Higher laser fluence may give greater nonlinear effect but with lower light-to-heat conversion efficiency.